Theor Chem Acc (2011) 130:815–828
DOI 10.1007/s00214-011-1045-2

REGULAR ARTICLE

Interference-induced electron- and hole-conduction asymmetry

Sören Wohlthat · Gemma C. Solomon · Noel S. Hush · Jeffrey R. Reimers

Received: 4 July 2011 / Accepted: 13 September 2011 / Published online: 5 October 2011

Abstract Principles established by Shephard and Paddon-Row for optimizing and controlling intramolecular electron transport through the modulation of interfering pathways are employed to design new molecules for steady-state conduction experiments aimed at manifesting electron–hole conduction asymmetry in a unique way. First, a review of the basic principles is presented through application to a pertinent model system in which a molecule containing donor and acceptor terminal linking groups with an internal multiple-pathway bridge is used to span two metal electrodes. Different interference patterns are produced depending on whether the through-molecule coupling pathways are symmetric or antisymmetric with respect to a topological bisecting plane, giving rise to asymmetric electron and hole conductances at the tight-binding (Hückel) level; this process is also described from a complementary molecular-orbital viewpoint. Subsequently, a new molecular system based on organic polyradicals is designed to allow such asymmetry to be realized in single-molecule conduction experiments. These polyradicals are analyzed using analogous simple models, density-functional theory (DFT) calculations of steady-state transmission, and intermediate neglect of differential overlap (INDO) calculations of intramolecular connectivity, verifying that polyradicals at low temperatures should show experimentally measureable electron–hole conduction asymmetry. A key feature of this system is that the polyradicals form a narrow partially occupied band of orbitals that lie within and well separated from the HOMO and LUMO orbitals of the surrounding molecular scaffold, allowing for holes and electrons to be transported through the same molecular band.

Keywords Single-molecule conductivity · Electron transfer · Interference · Polyradicals · Electron–hole conduction asymmetry

Dedicated to Professor Akira Imamura on the occasion of his 77th birthday and published as part of the Imamura Festschrift Issue.

Electronic supplementary material The online version of this article (doi:10.1007/s00214-011-1045-2) contains supplementary material, which is available to authorized users.

S. Wohlthat · N. S. Hush · J. R. Reimers (✉)
School of Chemistry, The University of Sydney, Sydney, NSW 2006, Australia
e-mail: jeffrey.reimers@sydney.edu.au

G. C. Solomon
Nano-Science Center and Department of Chemistry, University of Copenhagen, Universitetparken 5, 2100 Copenhagen Ø, Denmark

N. S. Hush
School of Molecular Bioscience, The University of Sydney, Sydney, NSW 2006, Australia

1 Introduction

Interferences caused by different pathways when electrons transfer from a donor to an acceptor through a bridge were much discussed during the 1980s–1990s [1–23]. Careful design of pathways paved the way for the synthesis of σ "superbridges" for intramolecular electron-transfer processes [24]; such processes are very important for the understanding of electron and energy transport in biology, through chemical systems, and in natural and artificial light-harvesting and solar-energy conversion processes. In recent times, the analysis of interferences between different pathways has been revived in the conduction analysis of single molecules connected to metallic electrodes offering, in principle, means by which molecular devices can be

controlled. The common underlying chemistry means that strong connections exist between these two research fields [25] and from early on techniques developed for electron-transfer reactions have been used to understand steady-state conductivity [26–31]. Much focus has been on the conduction of π-conjugated molecules and the use of orbital symmetry and substituent control over interferences [8, 32–76], and this field has been recently reviewed [77], including also a review in this issue [78] that is dedicated to Prof. Imamura's contributions to this field [79–90] and other aspects of Theoretical Chemistry.

Here, we focus on the through-σ-bridge odd/even pathway interference concept championed by Shephard and Paddon-Row [17, 24], applying it to explore a possible new class of interference processes in molecular electronic devices using both Ratner's Lippmann–Schwinger-based pathways approach [10] and molecular-orbital approaches. A most significant aspect of the original interference analysis was the prediction that the conduction of electrons and holes through the *same* tight-binding orbital band should be asymmetric. More generally, electron- and hole-conduction asymmetry is particularly relevant to many applications in superconductivity and graphene conductivity [91–100]. Based upon a standard Hückel tight-binding approach, symmetric conduction of electrons and holes is generally expected. While it is known that asymmetry can be introduced by two-electron interactions within molecules [91–95], junction effects [97], impurities [96, 100], substituents (see e.g. [98] for a modern graphene application) and stacking [99], Shephard and Paddon-Row [17, 24] showed that asymmetry can also be an exploitable intrinsic property of a single band manifested just at the one-electron tight-binding level. Normally, it is not manifest as most molecular experiments place the charge source and destination at energies between the molecular HOMO and LUMO orbitals, treating the individual occupied and virtual bands via effective individual band models: if the same Hückel parameters are used for each band, then no asymmetry arises. However, the theory predicts that if a band of partially occupied orbitals is placed energetically between the source and destination orbitals (with all of these surrounded by the primary occupied and virtual orbitals of the surrounding molecular scaffold), then hole and electron conduction through the *same* band can occur. In this circumstance, odd/even path-length interference effects are predicted to manifest as electron–hole conduction asymmetry.

In Sect. 2 the basic formalism for steady-state molecular conductivity is reviewed, while in Sect. 3 a basic model system for steady-state conductivity based on this scenario is introduced, akin to models used previously [17] for intramolecular electron transfer. This model system contains terminal groups linked through a molecular wire that facilitates the coherent transport of charge from one implicitly coupled electrode (lead) to another. Analytical solutions to the model are obtained detailing transport asymmetry, its origin in terms of interference effects, and other consequences of the interference such as modulations of molecular-orbital energies. Many of the well-known generic effects of interference and its manifestations are exposed by this analysis.

In Sect. 4 polyradicals are proposed as a realistic molecular system that could manifest Shephard/Paddon-Row type interference-controlled conductance in single-molecule conduction experiments: the isolated partially occupied band of radical orbitals lies in the middle of the HOMO-LUMO gap of the molecular scaffold [101], allowing for the possibility of hole conduction and electron conduction through the same orbitals. A basic system is developed and related to the simplest model described initially. DFT calculations of molecular structure and electron transmission between gold electrodes verify the basic properties and conduction asymmetry. Using a very different computational method, intermediate neglect of differential overlap (INDO), connection is re-established between the model and DFT conduction asymmetries and the intramolecular transport properties of the polyradicals. As these molecules are large and thermal motion and inelastic scattering can act to obscure selection rules and interferences [22, 23, 102–113], the results obtained pertain to low-temperature low-voltage experiments only.

2 Basic description of steady-state single-molecule conductivity

The current I at bias voltage V passing through a molecular conductor sandwiched between two electrodes (leads) A and B can be expressed using the Landauer formula [28, 31, 114–119] as

$$I(V) = \frac{e}{\pi\hbar} \int_{E_F - eV/2}^{E_f + eV/2} T(E,V)\mathrm{d}E, \tag{1}$$

where T is the transmission and the integral is over all electron energies E away from the Fermi energy E_f and is given by

$$T(E,V) = \mathbf{\Gamma}_B(E,V)\mathbf{G}_M(E,V)\mathbf{\Gamma}_A(E,V)\mathbf{G}_M^{\dagger}(E,V), \tag{2}$$

where $\mathbf{\Gamma}_A$ and $\mathbf{\Gamma}_B$ are twice the imaginary component of the self-energies of the electrodes interacting with the molecule via couplings $\mathbf{J}_A$ and $\mathbf{J}_B$, respectively,

$$\begin{aligned} &\mathbf{\Sigma}_A(E,V) = \mathbf{J}_A^{\dagger}(V)\mathbf{G}_A(E,V)\mathbf{J}_A(V) \quad \text{and} \\ &\mathbf{\Sigma}_B(E,V) = \mathbf{J}_B^{\dagger}(V)\mathbf{G}_B(E,V)\mathbf{J}_B(V); \end{aligned} \tag{3}$$

here, $\mathbf{G}_A$ and $\mathbf{G}_B$ are the unperturbed Green's functions of the electrodes and

$$G_{\mathrm{M}} = (z\mathbf{1} - \mathbf{H}(V) + \mathbf{\Sigma}_{\mathrm{A}}(E,V) + \mathbf{\Sigma}_{\mathrm{B}}(E,V))^{-1} \quad (4)$$

is the perturbed Green's function of the molecule, where $\mathrm{Re}(z) = E$ and $\mathbf{H}(V)$ is the Hamiltonian operator for the molecular part.

A priori computational methods such as non-equilibrium Green's function theory (NEGF) [116–119] solve for the electronic structure of the molecule experiencing a steady-state current using for example DFT, as we do in Sect. 4. Such approaches usually move the "electrode"–"molecule" junction into the metal, using "extended molecules" containing not just the organic component but also a significant number of attaching metal atoms, seeking convergence of the calculated properties with expansion of the extended molecule [120]. We employ 20-atom gold clusters attached to the organic molecules for this purpose [119]. However, using the wide-band approximation, the real components of the self-energies may be ignored and the imaginary components approximated by a constant $\mathbf{\Gamma}_{\mathrm{A}}(E, V) = \mathbf{\Gamma}_{\mathrm{B}}(E, V) = \Gamma$. Also, in simple models, the molecule can be replaced by an effective two-level system with the two levels coupled through an effective coupling:

$$\mathbf{H} = \begin{bmatrix} E_{\mathrm{D}} & H^{\mathrm{eff}} \\ H^{\mathrm{eff}} & E_{\mathrm{A}} \end{bmatrix}. \quad (5)$$

This is the same simplest-level description used historically to describe discrete electron-transfer events in molecules between donors (D) and acceptors (A), with interferences manifesting themselves through how the general molecular properties control the effective end-to-end coupling H^{eff}.

3 A simple model

Figure 1 shows a simple model for through molecule conduction and intramolecular electron transfer. It is comprised of a donor (D), acceptor (A), and four-site connecting bridge (1–4), with each represented by a single-site (atomic) orbital. For convenience, the onsite energies of sites 1–4 are set to zero. The couplings between these sites are taken to be $\beta_3 = \beta = -|\beta_2| = -0.08$ eV, and initially, we set $\beta_1 = \beta$; the inclusion of such a coupling between two otherwise independent paths is crucial to our analysis. With respect to a perpendicular mirror plane passing through the donor and acceptor sites, the couplings are symmetric (A′) for $\beta_2 = \beta$ and antisymmetric (A″) for $\beta_2 = -\beta$. Most real molecules have different sets of coupled orbitals, and the net conduction thus represents weighted sums from both types of couplings. We consider each type separately, however.

The transmission of the symmetrically coupled system (A′) acting as a linker between two metal electrodes assuming a connection between D or A and the electrodes of $\Gamma = -0.01$ eV is plotted in Fig. 2. In the off-resonant regime, the transmission of electrons (red dashed line) is larger than the transmission of holes (black solid line). This is the electron- and hole-conduction asymmetry that is discussed in the remainder of the paper. In Fig. 2, the transmission for the antisymmetrically (A″) coupled model is shown for comparison. We observe that the transmissions of holes and electrons are simply reversed compared to those of the A′ case.

Interference during electron transfer may be treated from the perspective of perturbations to the Hamiltonian matrix and its molecular orbitals or from a pathways perspective using either Green's function or Lippmann–Schwinger techniques, and these approaches have been established to be essentially equivalent [22, 121–123]; current-pathway techniques are also in modern use [124]. We use the Lippmann–Schwinger approach to consider interfering pathways through atomic orbitals and then also interfering pathways through molecular orbitals.

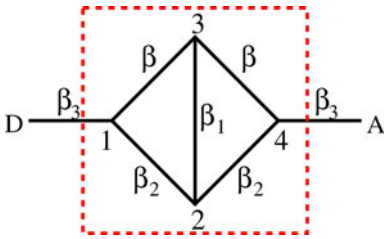

Fig. 1 A model system of a bridge coupling a donor (*D*) to an acceptor (*A*). The bridge consists of sites 1–4 inside the *red dashed square* and has inter-site couplings of β, β_1, β_2, and β_3. For $\beta_2 = \beta$, the couplings are symmetric (A′) with respect to the plane through D and A, while for $\beta_2 = -\beta$, they are antisymmetric (A″). We consider only $\beta_3 = \beta$

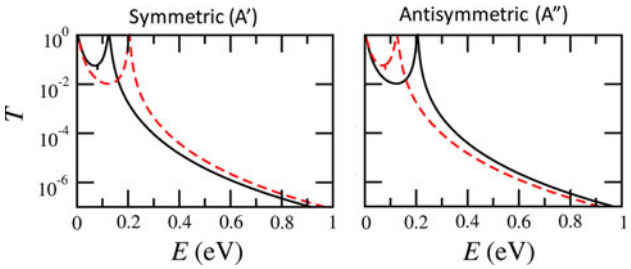

Fig. 2 Transmission *T* of the model displayed in Fig. 1. The donor and acceptor are assumed to be metallic electrodes in the wide-band approximation ($\Gamma = 0.01$ eV). $T(E)$ is plotted as the *black solid line* (holes), while $T(-E)$ is plotted as the red dashed line (electrons). The band centre is set to $E = 0$ eV

3.1 Interfering atomic-orbital pathways

First, the asymmetry produced by our simple model is analyzed in terms of interferences between different spatial pathways. To describe interferences of different pathways, Ratner introduced an iterative form of the Lippmann–Schwinger equation depicting the effective electronic coupling between two states, H_{ij}^{eff} [10]. The Hamiltonian is split into an unperturbed part H_0, which defines a basis of non-interacting states, and a perturbation V that mixes the non-interacting states

$$H = H_0 + V. \tag{6}$$

The effective coupling element between states i and j is expressed as

$$H_{ij}^{\text{eff}} = V_{ij} + \sum_k \frac{V_{ik} H_{kj}^{\text{eff}}}{E - E_k + i\eta}, \tag{7}$$

where V_{ij} is the coupling between the states i and j, E_k is the energy of state k, and η is an infinitesimal positive number that does not influence the nature of the asymptotic states of transported electrons or holes [125]. Iterative solution of Eq. 7 delivers a sum over all pathways connecting states i and j. If the denominators $E - E_k$ become large, we expect only a small number of short pathways to contribute significantly to the effective coupling.

In the basis set of localized orbitals (i.e., each site comprised either of a simple atomic orbital or of a "molecular" orbital taken from a localized molecular fragment) D, 1, 2, 3, 4, and A shown in Fig. 1, the two shortest pathways for conduction are D → 1 → 2 → 4 → A (pathway A) and D → 1 → 3 → 4 → A (pathway B). The two second-shortest pathways are D → 1 → 2 → 3 → 4 → A (pathway C) and D → 1 → 3 → 2 → 4 → A (pathway D). The effective couplings between donor and acceptor due to these pathways are

$$H_{\text{A}}^{\text{eff}} = \frac{V_{\text{D1}}}{E - E_1}\frac{V_{12}}{E - E_2}\frac{V_{24}}{E - E_4}V_{4\text{A}} = \frac{\beta^2\beta_2^2}{E^3} = \frac{\beta^4}{E^3} \tag{8}$$

$$H_{\text{B}}^{\text{eff}} = \frac{V_{\text{D1}}}{E - E_1}\frac{V_{13}}{E - E_3}\frac{V_{34}}{E - E_4}V_{4\text{A}} = \frac{\beta^4}{E^3} \tag{9}$$

$$H_{\text{C}}^{\text{eff}} = \frac{V_{\text{D1}}}{E - E_1}\frac{V_{12}}{E - E_2}\frac{V_{23}}{E - E_3}\frac{V_{34}}{E - E_4}V_{4\text{A}} = \frac{\beta^3\beta_1\beta_2}{E^4} = \pm\frac{\beta^4\beta_1}{E^4} \tag{10}$$

$$H_{\text{D}}^{\text{eff}} = \frac{V_{\text{D1}}}{E - E_1}\frac{V_{13}}{E - E_3}\frac{V_{32}}{E - E_2}\frac{V_{24}}{E - E_4}V_{4\text{A}} = \frac{\beta^3\beta_1\beta_2}{E^4} = \pm\frac{\beta^4\beta_1}{E^4} \tag{11}$$

as plotted in Fig. 3. The sign of the effective couplings due to pathways C and D depends on the symmetry of the couplings. It is + for A′ and − for A″. Assuming the symmetrically coupled model with β, $\beta_1 \leq 0$, the pathways interfere constructively for electron-like ($E < 0$) transport and destructively for hole-like ($E > 0$) transport. Thus, the pathway analysis explains the results of the transmissions shown in Fig. 2. For the antisymmetrically coupled model, the situation is reversed: hole-like transport interferes constructively and electron-like transport interferes destructively, as also depicted in Fig. 2.

The general scenario in which currents flowing through different types of paths (e.g., A′ and A″ coupled paths through say σ and π orbitals on the same atoms) has been proposed as a means for manifesting quantum interferences in molecular electronic devices. This can result in significant basis-set dependence of calculated currents [52, 59, 63, 68], especially if the interference is strong and/or if through-space conduction is significant. Interferences of this nature are not our primary concern, however, as we focus on the asymmetry of conduction of electrons and holes through each individual type of channel (A′ or A″).

3.2 Alternative interfering "molecular"-orbital picture

Looking at Fig. 2, one could think that the difference between electron- and hole-like transport arises from simply a shift of the energy with respect to the nearest molecular orbital, the "highest occupied molecular orbital" (HOMO) for holes or the "lowest unoccupied molecular orbital" (LUMO) for electrons, rather than from an interference feature. To examine this possibility more closely, we plot the transmission of the electrons reflected about the band centre, $T_{\text{A}'}(-E)$, and shifted so that the LUMO and the HOMO coincide, as shown in Fig. 4. The results show that the electronic transmissions especially close to these resonances are quite different from each other, and thus, the effect cannot be explained simply by the difference in energy to the nearest molecular orbital.

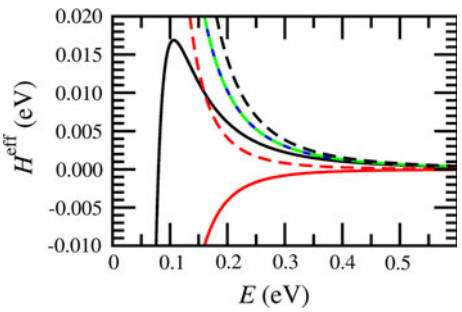

Fig. 3 Effective coupling for the symmetric model with $\beta_1 = \beta = -0.08$ eV in a localized orbital basis. *Solid lines* $H^{\text{eff}}(E)$; *dashed lines* $-H^{\text{eff}}(-E)$. *Blue* (*solid*), *green* (*dashed*): Path A + Path B. *Red*: Path C + Path D. *Black* Path A + Path B + Path C + Path D

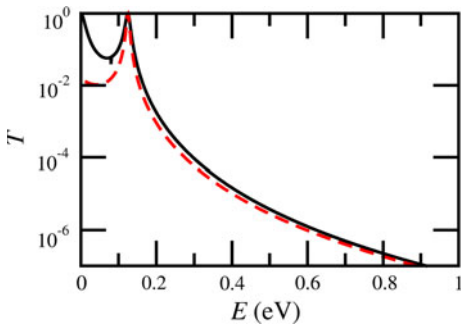

Fig. 4 Transmission T of the symmetric (A′) model displayed in Fig. 1. The donor and acceptor are assumed to be metallic electrodes in the wide-band approximation ($\Gamma = 0.01$ eV). $T_{A'}(E)$ is plotted as the *black solid line* (*holes*). $T_{A'}(-E+\beta_1)$ is plotted as the *red dashed line* (electrons)

To establish the connection between this molecular-orbital representation and that described earlier in terms of spatial interfering pathways, we analyze the model system further. We write down the Hamiltonian of the symmetrically coupled bridge with $\beta_2 = \beta$

$$H_{\text{Bridge}} = \begin{pmatrix} 0 & \beta & \beta & 0 \\ \beta & 0 & \beta_1 & \beta \\ \beta & \beta_1 & 0 & \beta \\ 0 & \beta & \beta & 0 \end{pmatrix}, \tag{12}$$

obtain its eigenvectors (see Supplementary Material) and eigenvalues

$$E_{\psi_1} = 0 \tag{13}$$

$$E_{\psi_2} = -\beta_1 \tag{14}$$

$$E_{\psi_3} = \frac{1}{2}\left(\beta_1 - \sqrt{16\beta^2 + \beta_1^2}\right) \tag{15}$$

$$E_{\psi_4} = \frac{1}{2}\left(\beta_1 + \sqrt{16\beta^2 + \beta_1^2}\right) \tag{16}$$

and plot the eigenvalues in Fig. 5 as a function of β_1. Increasing the magnitude of β_1 enables the interference pathways and causes the molecular orbitals ψ_3 and ψ_4 to shift. Molecular orbital ψ_2, which is not contributing to the transport because of its symmetry (see eigenvectors in the Supplementary Material), shifts in the opposite direction compared to ψ_3 and ψ_4 and thus ensures that the sum over the eigenvalues remains zero. For negative β_1, an incoming particle at $-E$ will be nearer in energy to the molecular orbitals contributing to transport while an incoming particle at $+E$ will be further removed from the bridge, leading to an increase in conduction for electrons and a decrease for holes for symmetric couplings, in agreement with predictions obtained directly based on pathway interference. For antisymmetric coupling, molecular orbitals ψ_3 and ψ_4 shift in the opposite direction compared to symmetric coupling (see Fig. 5), and thus, the conduction of electrons and holes is reversed.

Transforming the full Hamiltonian of the symmetrically coupled model including the terminal D and A orbitals

$$H_{\text{full}} = \begin{pmatrix} 0 & \beta & 0 & 0 & 0 & 0 \\ \beta & 0 & \beta & \beta & 0 & 0 \\ 0 & \beta & 0 & \beta_1 & \beta & 0 \\ 0 & \beta & \beta_1 & 0 & \beta & 0 \\ 0 & 0 & \beta & \beta & 0 & \beta \\ 0 & 0 & 0 & 0 & \beta & 0 \end{pmatrix} \tag{17}$$

into the basis set of the above bridge molecular orbitals gives

$$H_{\text{full}}^{\text{MO}} = \begin{pmatrix} 0 & -\frac{\beta}{\sqrt{2}} & 0 & \frac{1}{2}\beta\sqrt{1+\frac{\beta_1}{\sqrt{16\beta^2+\beta_1^2}}} & \frac{1}{2}\beta\sqrt{1-\frac{\beta_1}{\sqrt{16\beta^2+\beta_1^2}}} & 0 \\ -\frac{\beta}{\sqrt{2}} & 0 & 0 & 0 & 0 & \frac{\beta}{\sqrt{2}} \\ 0 & 0 & -\beta_1 & 0 & 0 & 0 \\ \frac{1}{2}\beta\sqrt{1+\frac{\beta_1}{\sqrt{16\beta^2+\beta_1^2}}} & 0 & 0 & \frac{1}{2}\left(\beta_1 - \sqrt{16\beta^2+\beta_1^2}\right) & 0 & \frac{1}{2}\beta\sqrt{1+\frac{\beta_1}{\sqrt{16\beta^2+\beta_1^2}}} \\ \frac{1}{2}\beta\sqrt{1-\frac{\beta_1}{\sqrt{16\beta^2+\beta_1^2}}} & 0 & 0 & 0 & \frac{1}{2}\left(\beta_1 + \sqrt{16\beta^2+\beta_1^2}\right) & \frac{1}{2}\beta\sqrt{1-\frac{\beta_1}{\sqrt{16\beta^2+\beta_1^2}}} \\ 0 & \frac{\beta}{\sqrt{2}} & 0 & \frac{1}{2}\beta\sqrt{1+\frac{\beta_1}{\sqrt{16\beta^2+\beta_1^2}}} & \frac{1}{2}\beta\sqrt{1-\frac{\beta_1}{\sqrt{16\beta^2+\beta_1^2}}} & 0 \end{pmatrix}. \tag{18}$$

We can analyze the effective couplings and compare to the atomic-orbital pathways. The shortest pathways through the system in the bridge molecular-orbital basis are

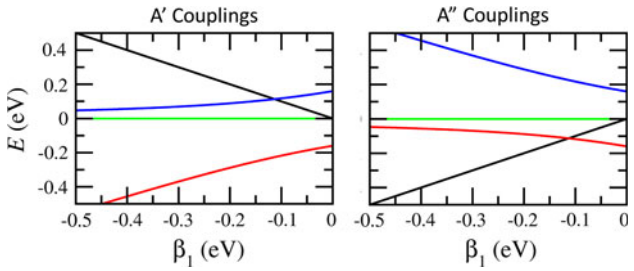

Fig. 5 Eigenvalues of the bridge. E_{ψ_1} is plotted in *green*. E_{ψ_2} in *black*, E_{ψ_3} in *red* and E_{ψ_4} is plotted in *blue*

$$H^{\text{eff}}_{\psi_1} = \frac{V_{\text{D}\psi_1}}{E - E_{\psi_1}} V_{\psi_1\text{A}} = -\frac{\beta^2}{2E} \tag{19}$$

$$H^{\text{eff}}_{\psi_2} = \frac{V_{\text{D}\psi_2}}{E - E_{\psi_2}} V_{\psi_2\text{A}} = 0 \tag{20}$$

$$H^{\text{eff}}_{\psi_3} = \frac{V_{\text{D}\psi_3}}{E - E_{\psi_3}} V_{\psi_3\text{A}} = \frac{\beta^2\left(1 + \frac{\beta_1}{\sqrt{16\beta^2+\beta_1^2}}\right)}{4\left[\frac{1}{2}\left(-\beta_1 + \sqrt{16\beta^2+\beta_1^2}\right) + E\right]} \tag{21}$$

$$H^{\text{eff}}_{\psi_4} = \frac{V_{\text{D}\psi_4}}{E - E_{\psi_4}} V_{\psi_4\text{A}} = \frac{\beta^2\left(1 - \frac{\beta_1}{\sqrt{16\beta^2+\beta_1^2}}\right)}{4\left[\frac{1}{2}\left(-\beta_1 - \sqrt{16\beta^2+\beta_1^2}\right) + E\right]} \tag{22}$$

as plotted in Fig. 6. If we expand these pathways around $E = \infty$, then

$$\begin{aligned} H^{\text{eff}}_{\psi_3} \approx {} & +\frac{\beta^2}{4E} + \frac{\beta^2\beta_1}{4\sqrt{16\beta^2+\beta_1^2}E} - \frac{2\beta^4}{\sqrt{16\beta^2+\beta_1^2}E^2} \\ & + \frac{\beta^4}{E^3} - \frac{\beta^4\beta_1}{\sqrt{16\beta^2+\beta_1^2}E^3} \\ & + \frac{\beta^4\beta_1}{E^4} - \frac{8\beta^6}{\sqrt{16\beta^2+\beta_1^2}E^4} - \frac{\beta^4\beta_1^2}{\sqrt{16\beta^2+\beta_1^2}E^4} \end{aligned} \tag{23}$$

$$\begin{aligned} H^{\text{eff}}_{\psi_4} \approx {} & +\frac{\beta^2}{4E} - \frac{\beta^2\beta_1}{4\sqrt{16\beta^2+\beta_1^2}E} + \frac{2\beta^4}{\sqrt{16\beta^2+\beta_1^2}E^2} \\ & + \frac{\beta^4}{E^3} + \frac{\beta^4\beta_1}{\sqrt{16\beta^2+\beta_1^2}E^3} \\ & + \frac{\beta^4\beta_1}{E^4} + \frac{8\beta^6}{\sqrt{16\beta^2+\beta_1^2}E^4} + \frac{\beta^4\beta_1^2}{\sqrt{16\beta^2+\beta_1^2}E^4}, \end{aligned} \tag{24}$$

and we find that $H^{\text{eff}}_{\psi_1} + H^{\text{eff}}_{\psi_3} + H^{\text{eff}}_{\psi_4} = H^{\text{eff}}_A + H^{\text{eff}}_B + H^{\text{eff}}_{\text{C}} + H^{\text{eff}}_{\text{D}}$ for large E. While in the molecular-orbital picture, pathways through different molecular orbitals interfere with each other, in the atomic-orbital picture spatial pathways interfere. Thus, as expected [22, 121–123], the two different basis sets lead to two different languages, languages that have both conceptual advantages and disadvantages for the description of system properties.

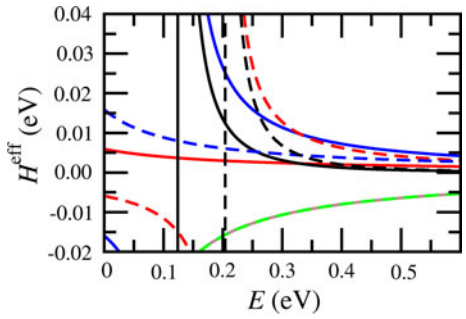

Fig. 6 Effective coupling for the symmetric model with $\beta_1 = \beta = \beta_2 = \beta_3 = -0.08$ eV. *Solid lines* $H^{\text{eff}}(E)$; *dashed lines* $-H^{\text{eff}}(-E)$. *Brown* (*solid*), *green* (*dashed*): $H^{\text{eff}}_{\psi_1}$. *Red* $H^{\text{eff}}_{\psi_3}$. *Blue* $H^{\text{eff}}_{\psi_4}$. *Black* $H^{\text{eff}}_{\psi_1} + H^{\text{eff}}_{\psi_3} + H^{\text{eff}}_{\psi_4}$

Figure 6 shows that close to a molecular orbital the pathway through that orbital dominates the effective coupling. Thus, the effective coupling near the LUMO can be described by the pathway due to orbital ψ_3 only and the effective coupling near the HOMO by the pathway due to orbital ψ_4 only. With the shifted energies $E' = E - E_{\psi_3}$ and $E'' = E - E_{\psi_4}$, the effective coupling near the LUMO is

$$H^{\text{eff}}_{\text{LUMO}} \approx \frac{\beta^2}{4E'}\left(1 + \frac{\beta_1}{\sqrt{16\beta^2+\beta_1^2}}\right) \tag{25}$$

and near the HOMO

$$H^{\text{eff}}_{\text{HOMO}} \approx \frac{\beta^2}{4E''}\left(1 - \frac{\beta_1}{\sqrt{16\beta^2+\beta_1^2}}\right). \tag{26}$$

From these results, we can see that it is β_1 that determines the difference in how fast the effective coupling, and thus, the transmission drops off around the frontier molecular orbital. For $\beta_1 < 0$, $H^{\text{eff}}_{\text{LUMO}}$ (electrons) drops off quicker than $H^{\text{eff}}_{\text{HOMO}}$ (holes) in agreement with the shifted transmission curves in Fig. 4.

While the above analysis was performed for the symmetrically coupled model system, analogous results are also obtained for the antisymmetrically coupled model, see Supplementary Material.

Interfering pathways through the bridge thus have *two* primary effects on conduction as viewed through a molecular-orbital picture: they redistribute the molecular-orbital energies within the band, and they change the effective couplings between the molecular orbitals and the external environment.

4 Application

To compare electron- and hole-like conduction in a single molecular system, it is desirable to have a molecular band that can be accessed from above and below in a single-molecule conduction experiment. The polyradicals shown in Fig. 7 are likely to display all required properties, with the radical orbitals expected to form a band lying in between the HOMO and LUMO orbitals of the surrounding molecular scaffold. Similar molecules have already been synthesized [126–129], and these new ones could possibly be synthesized using existing strategies [128, 129] starting from calix[6]arene instead of from calix[4]arene. The side group R in the meso position needs to be bulky to protect the radicals from associating. Typically 4-*tert*-butylphenyl groups or similar are used for this purpose; such substituents also limit the conformational flexibility of the rings and hence produce rigid, well-defined molecular structures. Most significantly, arylmethyl-based polyradicals are known to display intramolecular ferromagnetically coupled radicals resulting in high-spin states [126, 127, 130]. In an effective-single-electron picture, the electronic structure of these radicals is dominated by an occupied band of α-spins and an unoccupied band of β-spins localized at the radical sites. These bands are isolated inside the band gap between the major molecular occupied and virtual orbitals, making these ideal test candidates for a pathway-based conduction interference theory examining asymmetric electron and hole conduction through the same orbital band.

4.1 Hückel (tight-binding) model

To analyze the system, we reduce the molecules to a simple model as displayed in Fig. 8, with one localized orbital used to represent each bridge-radical site and each terminal-amine D or A group and only nearest-neighbor interactions are included. The molecular topologies arising from this model are shown in Fig. 9; these involve the essential element of interfering pathways considered previously based on the topology shown in Fig. 1. The nearest-neighbor couplings are taken to be -0.08 eV, and based on results obtained from DFT calculations, the onsite energy at the nitrogens is chosen to be -2.05 eV while those for α-spin and β-spin radical sites are set to -0.55 and 0.55 eV, respectively.

A significant feature of this model is that it represents the critical interactions with apparent D_{2h} symmetry whereas the molecules themselves have lower symmetry, either C_2 or C_i. In particular, the model Hamiltonians all have an additional symmetry plane perpendicular to the apparent "molecular" plane passing through both nitrogen orbitals, as did the model from Fig. 1, and again, we consider the couplings and "molecular orbitals" of the model Hamiltonian as being either symmetric (A′) or antisymmetric (A″) with respect to this plane.

Using the Landauer approach in the wide-band approximation (Eqs. 1–4, $\Gamma = 0.1$ eV) for the conductance of these molecules sandwiched between metal electrodes, the transmission through the nearest-neighbor model system is calculated assuming symmetric couplings and the results are plotted as dashed lines in the top panel of Fig. 10 for compound 1. At -2.05 eV, a peak due to the amine orbital appears, followed by three peaks corresponding to the benzene-like symmetric (A′) hexaradical's molecular orbitals; the peaks for α-spin are close to -0.5 eV, while those for β-spins are close to 0.5 eV. Similar results for antisymmetrically coupled orbitals are also shown in the middle panel of this figure, this time

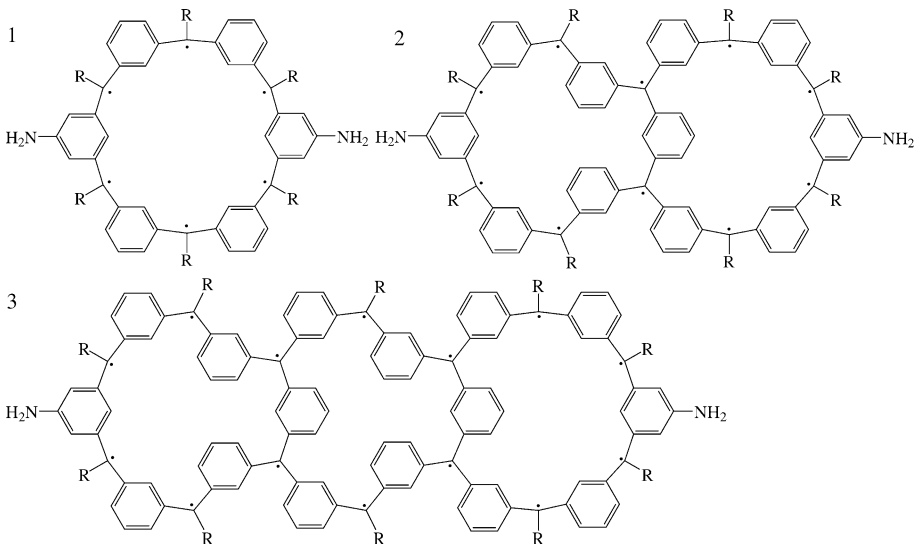

Fig. 7 Molecules: (*1*) hexaradical, (*2*) decaradical, (*3*) tetradecaradical. While synthesized molecules would most likely contain bulky substituents such as R=4-*tert*-butylphenyl, R=H is used in all calculations at compatible ring conformations

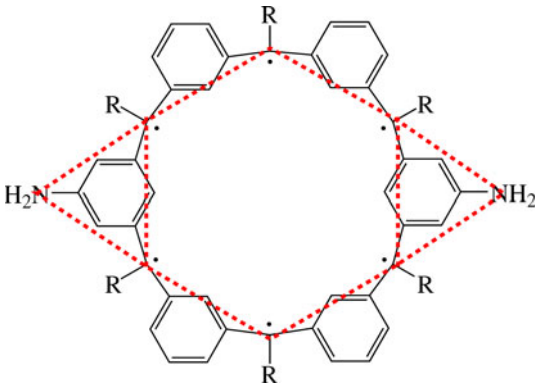

Fig. 8 From molecule to model. The isolated band formed by the radicals and coupled to the amines is modeled by the benzene-like hexaradical coupled to single orbitals on the amine group. The effective model topology is shown as the *red dotted figure*

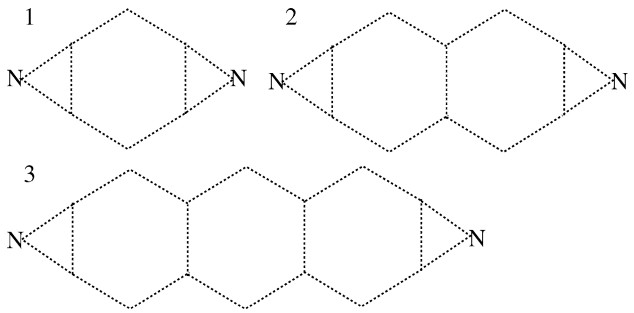

Fig. 9 Models: (*1*) benzene-like hexaradical, (*2*) naphthalene-like decaradical, (*3*) anthracene-like tetradecaradical

encompassing the three A″ benzene-like bridge orbitals. Most significantly, we see that the effects of interference on molecular-orbital energies, effective electrode couplings, and the transmission follow the same general scenario described earlier for the basic model system in Fig. 1.

The sum of the antisymmetric and symmetric models is provided in the lower panel of Fig. 10 to highlight that there exist only four unique bridge peaks as the two central peaks are degenerate. Sums such as this will contribute to the transmission through the actual molecules as paths through say atomic *s* and *p* orbitals on the amine groups are likely to have opposite symmetry properties. However, the weights of each type of path will not in general be equal, with, for example, amines supporting symmetric channels more than antisymmetric ones [131], and therefore, the symmetric ring states should couple more strongly; an example of a mix involving stronger A′ coupling is given in Fig. 1b of the Supplementary Material. When the weights become similar, basis-set and other effects can become critical in numerical calculations [52, 59, 68], but this situation is not appropriate for these molecules.

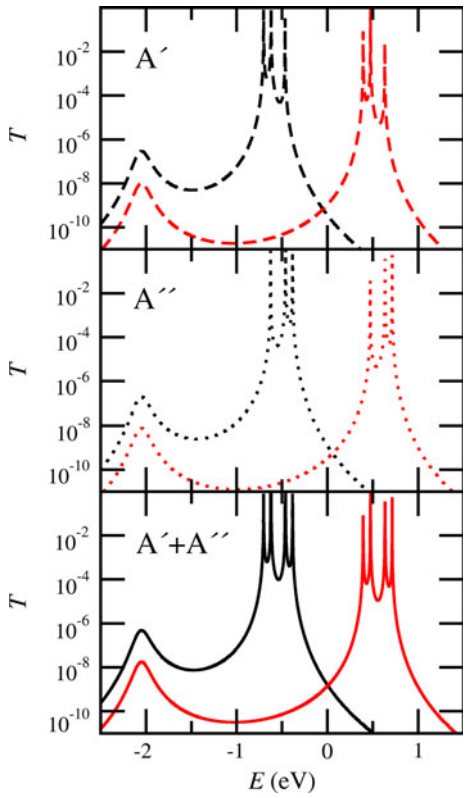

Fig. 10 Transmission through compound 1. *Black* α-spin. *Red* β-spin. *Dashed* symmetric orbitals. *Dotted* antisymmetric orbitals. *Solid* sum of symmetric and antisymmetric transmissions

4.2 DFT-calculated electronic transmissions through the full molecules

The geometries of compounds 1–3 with R=H (in configurations consistent with those expected for R=4-*tert*-butylphenyl) were optimized at the level of B3LYP/6-31G* using Gaussian [132], and the transmission of this molecule sandwiched between gold electrodes was calculated at the BP86/SVP level using Turbomole [133, 134] in combination with Green's function techniques (Eqs. 1–4, as detailed elsewhere [119]. This involves optimizing the molecules tethered to 4-layer 20-atom gold pyramids, the back two rows of which are frozen at a geometry to allow smooth interfacing to bulk gold; it has been shown to quantitatively reproduce experimental values for the conductances of molecules tethered to gold via amine linkers [131], as well being able to model hybridization [135] and interference effects [48] in such systems. All optimized structures are shown in Fig. 11 with coordinates provided in Supplementary Material, along with that for the next-longest member of the series containing four rings; these structures reveal how this molecular architecture can deliver an expandable pseudo-1-dimensional conductor. The calculated transmission for compound 1 is given in

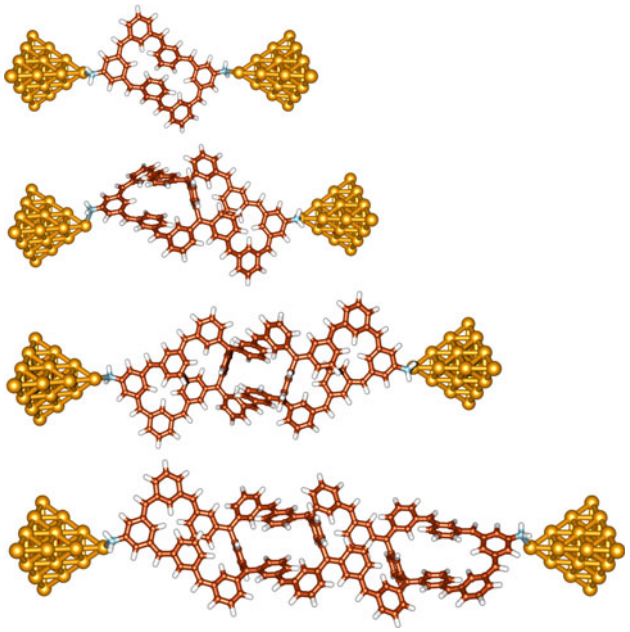

Fig. 11 Optimized molecular geometries at the level of DFT for polyradicals containing 1–4 rings

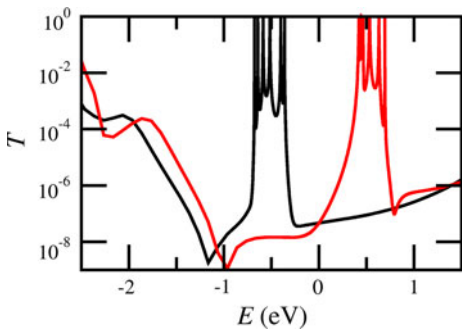

Fig. 12 Transmission through compound 1 calculated with DFT. *Black* α-spin. *Red* β-spin

Fig. 12 and appears similar to that for the sum of the symmetrically coupled and antisymmetrically coupled model systems, with peaks near −2.0 eV for the amine orbitals and bands at −0.5 eV for α-spins and at 0.5 eV for β-spins. Since the DFT calculations include all orbitals not just those on the radical sites, there are other bands that start to appear at the edges of the diagram. Nevertheless, the radical bands are roughly 1 eV away from any of the other bands and are thus fairly well isolated, establishing that, indeed, the polyradicals present an excellent system for the examination of interference effects.

As shown by Shephard and Paddon-Row [17] for this type of system, interferences between pathways influence the exponential decay of the transmission with respect to the length of the bridge which is increased in compounds 2 and 3. The optimized geometries are displayed in Fig. 11, alongside an optimized geometry for the same type of structure extended to four macrocycles. The transmissions for polyradicals 1–3 have been calculated using both the simple model and DFT at energies 0.5 eV above (for α-spin) and below (for β-spin) the band centres. In a through-molecule conduction experiment, gate electrodes can be used to set the alignment of the molecular orbitals and electrode Fermi energy, facilitating analogous measurements to be made. Here, the band centers were taken as the average of the peak positions of each band, which leads to transmissions evaluated roughly in the centre between the two bands. Therefore, the influence of the non-radical orbitals should be similar for both α- and β-spin transmissions and the resulting transmissions are plotted in Fig. 13, and exponential fits to their decay are listed in Table 1.

The results show that the exponential decay of hole transport (α-spins) is faster in the symmetrically coupled model system than in the antisymmetric one, while in the case of electron transport (β-spins), the results are reversed. These results are expected based on the interference patterns of the simple model sketched in Fig. 1 and are logical extensions of the work by Shephard and Paddon-Row [17]. If we equally sum transmissions of the symmetrically and antisymmetrically coupled models, there is almost no difference in the exponential decay of electrons and holes, i.e., the two contributions to conduction asymmetry cancel each other. However, if we assume that amines couple more strongly to the symmetric modes, we expect a faster decay for holes than for electrons; while the ratio of the two types of paths will be dependent on the precise nature of the interface geometry, this assumption is generally expected to hold. This faster decay is observed in the explicit DFT calculations for the polyradicals, establishing the results predicted by the interference model. While the calculated asymmetries are small, they are feasibly measureable, and the investigated voltage of 0.5 V from the band center is

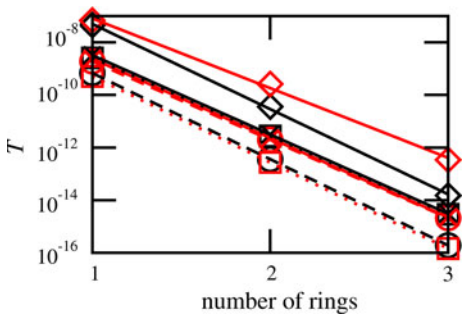

Fig. 13 Transmission at ±0.5 eV from the band centres. *Dashed line* and *circles* correspond to the model with symmetric coupling; *dotted line* and *squares* refer to the model with antisymmetric coupling; *solid line* and crosses show the sum of the symmetric and antisymmetric models. α-spin results are *black*; β-spin results are *red*. The *solid lines* connecting the diamonds indicate the DFT results. All *lines* are exponential fits, which are given in Table 1

Table 1 Exponential fits to the decays of the transmissions at $E = \pm 0.5$ eV with the number of rings n

Type	Spin	Fit	Symbol	Line style
A′	α	$1.2663 \times 10^{-6}\, e^{-7.5358n}$	Circle	Dashed
A′	β	$1.7883 \times 10^{-6}\, e^{-6.8537n}$	Circle	Dashed
A″	α	$2.4562 \times 10^{-6}\, e^{-6.8537n}$	Square	Dotted
A″	β	$9.5451 \times 10^{-7}\, e^{-7.5358n}$	Square	Dotted
A′ + A″	α	$3.3391 \times 10^{-6}\, e^{-6.9373n}$	Crosses	Solid
A′ + A″	β	$2.4546 \times 10^{-6}\, e^{-6.9398n}$	Crosses	Solid
DFT	α	$8.5956 \times 10^{-5}\, e^{-7.4521n}$	Diamond	Solid
DFT	β	$3.5748 \times 10^{-5}\, e^{-6.0959n}$	Diamond	Solid

The fits are plotted in Fig. 13

conservatively chosen to satisfy possible experimental challenges; however, as Fig. 1 demonstrates, the magnitude of the asymmetry should increase significantly at conduction voltages closer to resonance.

4.3 INDO-calculated couplings to external gold atoms

As interference effects between different pathways were first discovered for intramolecular charge-transfer processes, we consider also the properties of molecular complexes formed by adding single gold atoms to each nitrogen atom of the polyradicals. These complexes also provide simple models for the full steady-state conduction simulations described above. Most important are the effective couplings determined from the splittings of the two-valence Au *s*-orbitals in the complexes, and these are evaluated using restricted open-shell INDO calculations [136, 137], with the open-shell set to include both the organic radical orbitals and the Au *s*-orbitals. Through the variation in the INDO parameter I_{ss}, the Au *s*-orbitals are artificially positioned 0.50 eV above or below the band centre to mimic the previous Hückel and DFT steady-state conductance calculations.

The results are shown in Fig. 14, except for the splitting depicting hole transfer through molecule 3 as this is calculated to be less than 10^{-8} eV, which is the accuracy limit of the program. Exponential fits to the effective couplings are

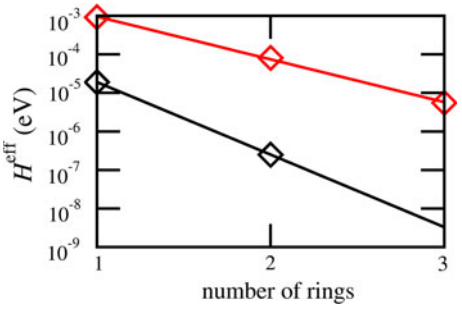

Fig. 14 Effective coupling between two Au *s*-orbitals calculated using restricted open-shell INDO

$$H_{\mathrm{e}}^{\mathrm{eff}} = 0.012248\,\mathrm{eV}\, e^{-2.5552n} \tag{27}$$

for electrons and

$$H_{\mathrm{h}}^{\mathrm{eff}} = 0.001444\,\mathrm{eV}\, e^{-4.3307n} \tag{28}$$

for holes. Since the effective couplings enter Fermi's golden rule expression for kinetic and transport coefficients as $|H^{\mathrm{eff}}|^2$, the exponents of the transfer rate obtained with INDO are roughly -5.1 eV for electrons and -8.7 eV for holes. Thus, the qualitative trend that electrons interfere less destructively than holes in these compounds is indicated in these INDO intramolecular electron-transfer calculations as well as in the DFT calculations of steady-state conduction. Indeed, a close relationship between steady-state conductivity and electron transfer is expected [25] and established analytically for the symmetrically coupled model system in the Supplementary Material.

5 Conclusions

Controlling the interference effects coming from different through-molecule coupling pathways has been an important tool for intramolecular electron and energy transfer as well as for steady-state conduction. We establish another link connecting the intramolecular pathways interference effects demonstrated by Shephard and Paddon-Row with electron–hole steady-state conduction asymmetry. Two equal and opposite types of interference effects are demonstrated, depending on the signs of the couplings linking equivalent donor to acceptor paths. These effects reorganize the molecular energy levels of the bridge and change their effective couplings to the electrodes, resulting in asymmetric conduction of electrons and holes. In actual molecules, couplings involving both symmetries are in general expected to occur, through, e.g., transmission through atomic *s*- and *p*-orbitals on key centers, hence reducing asymmetry to some extent.

Polyradicals are proposed as molecules that would show asymmetric electron and hole conduction through the *same* orbital band in single-molecule conduction experiments.

DFT calculations verify that these molecules contain occupied and unoccupied radical bands that form in the band-gap between the classic molecular bonding and antibonding orbitals, allowing their access for conductance in three-terminal single-molecule conduction experiments. These calculations verify the expected conduction asymmetry.

Based on the results for bridge-length dependencies determined for intramolecular electron transport, significantly different attenuation rates are expected for electron and hole transport through the polyradicals. DFT and model calculations verify this prediction, whilst INDO calculations demonstrate the direct connection between this effect and intramolecular couplings.

Acknowledgments We thank the National Computational Infrastructure (NCI) for providing computing resources and the Australian Research Council (ARC). G.C.S. acknowledges funding from The Danish Council for Independent Research|Natural Sciences.

References

1. Larsson S (1981) Electron transfer in chemical and biological systems. Orbital rules for nonadiabatic transfer. J Am Chem Soc 103:4034–4040
2. Beratan DN, Hopfield JJ (1984) Calculation of electron tunneling matrix elements in rigid systems: mixed-valence dithiaspirocyclobutane molecules. J Am Chem Soc 106:1584–1594
3. Mikkelsen KV, Ratner MA (1987) Electron tunneling in solid-state electron-transfer reactions. Chem Rev 87:113–153
4. Joachim C (1987) Ligand-length dependence of the intramolecular electron transfer through-bond coupling parameter. Chem Phys 116:339
5. Onuchic JN, Beratan DN (1987) Molecular bridge effects on distant charge tunneling. J Am Chem Soc 109:6771–6778
6. Beratan DN, Onuchic JN, Hopfield JJ (1987) Electron tunneling through covalent and noncovalent pathways in proteins. J Chem Phys 86:4488–4498
7. Rendell APL, Bacskay GB, Hush NS (1988) Electron transfer via dithiaspiroalkane linkages. Nature of long-range through-bond electronic coupling in disulfoxide radical cations and bis(metal) complexes and implications for the characterization of the SO bond. J Am Chem Soc 110:8343
8. Sautet P, Joachim C (1988) Electronic interference produced by a benzene embedded in a polyacetylene chain. Chem Phys Lett 153:511–516
9. Reimers JR, Hush NS (1989) Electron and energy transfer through bridged systems. I. Formalism. Chem Phys 134:323
10. Ratner MA (1990) Bridge-assisted electron transfer: effective electronic coupling. J Phys Chem 94:4877–4883
11. Reimers JR, Hush NS (1990) Electron and energy transfer through bridged systems. II. Tight binding linkages with zero asymmetric band gap. Chem Phys 146:89
12. Onuchic JN, De Andrade PCP, Beratan DN (1991) Electron tunneling pathways in proteins: a method to compute tunneling matrix elements in very large systems. J Chem Phys 95:1131–1138
13. Reimers JR, Hush NS (1994) Electron and energy transfer through bridged systems. III. Tight binding linkages with finite asymmetric band gap. J Photochem Photobiol A 82:31
14. Paulson BP, Curtiss LA, Bal B, Closs GL, Miller JR (1996) Investigation of through-bond coupling dependence on spacer structure. J Am Chem Soc 118:378–387
15. Skourtis SS, Onuchic JN, Beratan DN (1996) A method to analyze multi-pathway effects on protein mediated donor-acceptor coupling interactions. Inorg Chim Acta 243:167–175
16. Jordan KD, Paddon-Row MN (1992) Analysis of the interactions responsible for long-range through-bond-mediated electronic coupling between remote chromophores attached to rigid polynorbornyl bridges. Chem Rev 92:395
17. Shephard MJ, Paddon-Row MN (1995) Application of the parity rule of through-bond coupling to the design of "superbridges" that exhibit greatly enhanced electronic coupling. J Phys Chem 99:17497–17500
18. Liang C, Newton MD (1992) Ab initio studies of electron transfer: pathway analysis of effective transfer integrals. J Phys Chem 96:2855
19. Naleway CA, Curtiss LA, Miller JR (1991) Superexchange-pathway model for long-distance electronic couplings. J Phys Chem 95:8434
20. Shephard MJ, Paddon-Row MN, Jordan KD (1994) Why is a simple n-alkyl bridge more efficient than a polynorbornyl bridge at mediating through-bond coupling? J Am Chem Soc 116:5328–5333
21. Newton MD (1999) Control of electron transfer kinetics: models for medium reorganization and donor-acceptor coupling. Adv Chem Phys 106:303–375
22. Skourtis SS, Beratan DN (1999) Theories of structure-function relationships for bridge-mediated electron transfer reactions. Adv Chem Phys 106:377–452
23. Regan JJ, Onuchic JN (1999) Electron-transfer tubes. Adv Chem Phys 107:497–553
24. Paddon-Row MN, Shephard MJ (1997) Through-bond orbital coupling the parity rule and the design of "Superbridges" which exhibit greatly enhanced electronic coupling: a natural bond orbital analysis. J Am Chem Soc 119:5355
25. Nitzan A (2001) A relationship between electron-transfer rates and molecular conduction. J Phys Chem A 105:2677
26. Cheong A, Roitberg AE, Mujica V, Ratner MA (1994) Resonances and interference effects on the effective electronic coupling in electron transfer. J Photochem Photobio A 82:81–86
27. Mujica V, Kemp M, Ratner MA (1994) Electron conduction in molecular wires. II. Application to scanning tunneling microscopy. J Chem Phys 101:6856–6864
28. Mujica V, Kemp M, Ratner MA (1994) Electron conduction in molecular wires. I. A scattering formalism. J Chem Phys 101:6849–6855
29. Yaliraki SN, Roitberg AE, Gonzalez C, Mujica V, Ratner MA (1999) The injecting energy at molecule/metal interfaces: implications for conductance of molecular junctions from an ab initio molecular description. J Chem Phys 111:6997–7002
30. Mujica V, Nitzan A, Mao Y, Davis W, Kemp M, Roitberg A, Ratner MA (1999) Electron transfer in molecules and molecular wires: geometry dependence, coherent transfer, and control. Adv Chem Phys 107:403–429
31. Hall LE, Reimers JR, Hush NS, Silverbrook K (2000) A priori Green's-function-based calculations of current-voltage characteristics of molecular wires. J Chem Phys 112:1510
32. Patoux C, Coudret C, Launay JP, Joachim C, Gourdon A (1997) Topological effects on intramolecular electron transfer via quantum interference. Inorg Chem 36:5037–5049
33. Emberly EG, Kirczenow G (1999) Antiresonances in molecular wires. J Phys Condens Matter 11:6911–6926
34. Lee HW (1999) Generic transmission zeros and in-phase resonances in time-reversal symmetric single channel transport. Phys Rev Lett 82:2358–2361

35. Baer R, Neuhauser D (2002) Phase coherent electronics: a molecular switch based on quantum interference. J Am Chem Soc 124:4200–4201
36. Mayor M, Weber HB, Reichert J, Elbing M, Von Hänisch C, Beckmann D, Fischer M (2003) Electric current through a molecular rod—relevance of the position of the anchor groups. Angew Chem Int Ed 42:5834–5838
37. Stadler R, Forshaw M, Joachim C (2003) Modulation of electron transmission for molecular data storage. Nanotechnology 14:138–142
38. Stadler R, Ami S, Joachim C, Forshaw M (2004) Integrating logic functions inside a single molecule. Nanotechnology 15:S115–S121
39. Walter D, Neuhauser D, Baer R (2004) Quantum interference in polycyclic hydrocarbon molecular wires. Chem Phys 299:139–145
40. Ernzerhof M, Zhuang M, Rocheleau P (2005) Side-chain effects in molecular electronic devices. J Chem Phys 123:134704/1–134704/5
41. Stadler R, Thygesen KS, Jacobsen KW (2005) An ab initio study of electron transport through nitrobenzene: the influence of leads and contacts. Nanotechnology 16:S155–S160
42. Cardamone DM, Stafford CA, Mazumdar S (2006) Controlling quantum transport through a single molecule. Nano Lett 6:2422–2426
43. Papadopoulos TA, Grace IM, Lambert CJ (2006) Control of electron transport through Fano resonances in molecular wires. Phys Rev B Condens Matter Mater Phys 74:193306
44. Ernzerhof M (2007) A simple model of molecular electronic devices and its analytical solution. J Chem Phys 127:204709
45. Stafford CA, Cardamone DM, Mazumdar S (2007) The quantum interference effect transistor. Nanotechnology 18:424014
46. Maiti SK (2007) Quantum transport through polycyclic hydrocarbon molecules. Phys Lett A 366:114–119
47. Solomon GC, Andrews DQ, Goldsmith RH, Hansen T, Wasielewski MR, Van DRP, Ratner MA (2008) Quantum interference in acyclic systems: conductance of cross-conjugated molecules. J Am Chem Soc 130:17301–17308
48. Wohlthat S, Pauly F, Reimers JR (2008) Two-dimensional phenanthroline-based extended pi-conjugated molecules for single-molecule conduction. J Phys Condens Matter 20:295208
49. Andrews DQ, Solomon GC, Goldsmith RH, Hansen T, Wasielewski MR, Van Duyne RP, Ratner MA (2008) Quantum interference: the structural dependence of electron transmission through model systems and cross-conjugated molecules. J Phys Chem C 112:16991–16998
50. Andrews DQ, Solomon GC, Van Duyne RP, Ratner MA (2008) Single molecule electronics: increasing dynamic range and switching speed using cross-conjugated species. J Am Chem Soc 130:17309–17319
51. Fowler PW, Pickup BT, Todorova TZ (2008) Equiconducting molecular conductors. Chem Phys Lett 465:142–146
52. Ke S-H, Yang W, Baranger HU (2008) Quantum-interference-controlled molecular electronics. Nano Lett 8:3257–3261
53. Pickup BT, Fowler PW (2008) An analytical model for steady-state currents in conjugated systems. Chem Phys Lett 459:198–202
54. Solomon GC, Andrews DQ, Hansen T, Goldsmith RH, Van Duyne RP, Ratner MA (2008) Understanding quantum interference in coherent molecular conduction. J Chem Phys 129:054701
55. Solomon GC, Andrews DQ, van Duyne RP, Ratner MA (2008) When things are not as they seem: quantum interference turns molecular electron transfer "Rules" upside down. J Am Chem Soc 130:7788–7789
56. Yoshizawa K, Tada T, Staykov A (2008) Orbital views of the electron transport in molecular devices. J Am Chem Soc 130:9406–9413
57. Fowler PW, Pickup BT, Todorova TZ, Pisanski T (2009) Fragment analysis of single-molecule conduction. J Chem Phys 130:174708
58. Hansen T, Solomon GC, Andrews DQ, Ratner MA (2009) Interfering pathways in benzene: an analytical treatment. J Chem Phys 131:194704
59. Solomon GC, Andrews DQ, Van Duyne RP, Ratner MA (2009) Electron transport through conjugated molecules: when the pi system only tells part of the story. Chem Phys Chem 10:257–264
60. Stadler R (2009) Quantum interference effects in electron transport through nitrobenzene with pyridil anchor groups. Phys Rev B Condens Matter Mater Phys 80:125401
61. Tsuji Y, Staykov A, Yoshizawa K (2009) Orbital control of the conductance photoswitching in diarylethene. J Phys Chem C 113:21477–21483
62. Tsuji Y, Staykov A, Yoshizawa K (2009) Orbital view concept applied on photoswitching systems. Thin Solid Films 518:444–447
63. Herrmann C, Solomon GC, Subotnik JE, Mujica V, Ratner MA (2010) Ghost transmission: how large basis sets can make electron transport calculations worse. J Chem Phys 132:024103/1–024103/17
64. Li X, Staykov A, Yoshizawa K (2010) Orbital views of the electron transport through polycyclic aromatic hydrocarbons with different molecular sizes and edge type structures. J Phys Chem C 114:9997–10003
65. Rincon J, Hallberg K, Aligia AA, Ramasesha S (2009) Quantum interference in coherent molecular conductance. Phys Rev Lett 103:266807
66. Liu H, Ni W, Zhao J, Wang N, Guo Y, Taketsugu T, Kiguchi M, Murakoshi K (2009) Nonequilibrium Green's function study on the electronic structure and transportation behavior of the conjugated molecular junction: terminal connections and intramolecular connections. J Chem Phys 130:244501
67. Herrmann C, Solomon GC, Ratner MA (2010) Local pathways in coherent electron transport through iron porphyrin complexes: a challenge for first-principles transport calculations. J Phys Chem C 114:20813–20820
68. Markussen T, Schiotz J, Thygesen KS (2010) Electrochemical control of quantum interference in anthraquinone-based molecular switches. J Chem Phys 132:224104
69. Ricks AB, Solomon GC, Colvin MT, Scott AM, Chen K, Ratner MA, Wasielewski MR (2010) Controlling electron transfer in donor-bridge-acceptor molecules using cross-conjugated bridges. J Am Chem Soc 132:15427–15434
70. Saha KK, Nikolic BK, Meunier V, Lu W, Bernholc J (2010) Quantum-interference-controlled three-terminal molecular transistors based on a single ring-shaped molecule connected to graphene nanoribbon electrodes. Phys Rev Lett 105:236803
71. Solomon GC, Herrmann C, Vura-Weis J, Wasielewski MR, Ratner MA (2010) The chameleonic nature of electron transport through pi-stacked systems. J Am Chem Soc 132:7887–7889
72. Solomon GC, Vura-Weis J, Herrmann C, Wasielewski MR, Ratner MA (2010) Understanding coherent transport through pi-stacked systems upon spatial dislocation. J Phys Chem B 114:14735–14744
73. Yang H, Mayne AJ, Boucherit M, Comtet G, Dujardin G, Kuk Y (2010) Quantum interference channeling at graphene edges. Nano Lett 10:943–947
74. Fracasso D, Valkenier H, Hummelen JC, Solomon GC, Chiechi RC (2011) Evidence for quantum interference in SAMs of

arylethynylene thiolates in tunneling junctions with Eutectic Ga-In (EGaIn) top-contacts. J Am Chem Soc 133:9556–9563
75. Solomon GC, Andrews DQ, Ratner MA (2011) Quantum interference in acyclic molecules. In: Siebbeles LDA, Grozema FC (eds) Charge and exciton transport through molecular wires. Wiley, London, pp 19–59
76. Tsuji Y, Staykov A, Yoshizawa K (2011) Orbital views of molecular conductance perturbed by anchor units. J Am Chem Soc 133:5955–5965
77. Markussen T, Stadler R, Thygesen KS (2010) The relation between structure and quantum interference in single molecule junctions. Nano Lett 10:4260–4265
78. Li X, Staykov A, Yoshizawa K (2011) Orbital views of the electron transport through heterocyclic aromatic hydrocarbons. Theor Chem Acc. doi:10.1007/s00214-011-0968-y
79. Naraba T, Mizushima Y, Noake H, Imamura A, Igarashi Y, Torihashi Y, Nishioka A (1965) Preparation and electrical properties of poly(tetracyanoethylene) copper chelate film. Jpn J Appl Phys 4:977–986
80. Naraba T, Mizushima Y, Noake H, Nishioka A, Igarashi Y, Imamura A, Torihashi Y (1967) Preparation and electrical properties of poly(tetracyanoethylene copper chelate) film. Rev Electr Commun Lab 15:551–562
81. Yamabe T, Tanaka K, Teramae H, Fukui K, Imamura A, Shirakawa H, Ikeda S (1979) Electronic properties of pure and doped polyacetylenes. J Phys C 12:L257–L262
82. Seki K, Tanaka H, Ohta T, Aoki Y, Imamura A, Fujimoto H, Yamamoto H, Inokuchi H (1990) Electronic structure of poly(tetrafluoroethylene) studied by UPS, VUV absorption, and band calculations. Phys Scr 41:167–171
83. Imamura A, Aoki Y, Nishimoto K, Kurihara Y, Nagao A (1994) Calculations of the electronic structure of various aperiodic polymers by an elongation method. Int J Quant Chem 52:309–319
84. Tada T, Aoki Y, Imamura A (1998) The contributions of chalcogen to the Peierls instability in model crystals of charge-transfer complexes. Synth Met 95:169–177
85. Imamura A (1999) Molecular orbital calculations of pi-electron conjugated polymers. Kobunshi 48:336
86. Imamura A, Aoki Y (2003) Method of controlling electric conductivity by modifying both terminals of compounds containing polyyne chains. Japan Patent JP2003016120A, 17 Jan 2003
87. Imamura A, Aoki Y (2003) Parallel and layered structure process for efficient calculation of electronic state of giant molecules. Japan Patent JP2003012567A, 15 Jan 2003
88. Ohnishi S, Gu FL, Naka K, Imamura A, Kirtman B, Aoki Y (2004) Calculation of static (hyper)polarizabilities for pi-conjugated donor/acceptor molecules and block copolymers by the elongation finite-field method. J Phys Chem A 108:8478–8484
89. Tada T, Aoki Y, Imamura A (2004) An analytical molecular orbital approach in tetrathiafulvalene tetracyanoquinodimethane (TTF-TCNQ). Mol Phys 102:1891–1901
90. Imamura A, Aoki Y (2006) Molecular design of a pi-conjugated single-chain electronically conductive polymer. Int J Quant Chem 106:1924–1933
91. Gagliano ER, Avignon M (1994) Electron-hole asymmetry in a generalized one-band Hubbard model. In: Noce C, Romano A, Scarpetta G (eds) Superconductivity and strongly correlated electron systems. World Scientific, Singapore, pp 226–240
92. Zaitsev RO, Mikhailova YV (1996) The electron-hole asymmetry of high temperature superconductors. Fiz Nizk Temp (Kiev) 22:510–514
93. Hirsch JE (2003) Electron-hole asymmetry is the key to superconductivity. Int J Mod Phys B 17:3236–3241
94. Kobayashi A, Tsuruta A, Matsuura T, Kuroda Y (2004) Origins of electron-hole asymmetry in cuprate superconductors. J Magn Magn Mater 272–276:E187–E188
95. Maciag A, Wrobel P (2006) Asymmetric tunneling conductance in doped antiferromagnets. Acta Phys Pol A 109:607–610
96. Hwang EH, Adam S, Das SS (2007) Carrier transport in two-dimensional graphene layers. Phys Rev Lett 98:186806
97. Han W, Wang WH, Pi K, McCreary KM, Bao W, Li Y, Miao F, Lau CN, Kawakami RK (2009) Electron-hole asymmetry of spin injection and transport in single-layer graphene. Phys Rev Lett 102:137205
98. Fan X-Y, Nouchi R, Yin L-C, Tanigaki K (2010) Effects of electron-transfer chemical modification on the electrical characteristics of graphene. Nanotechnology 21:475208
99. Mucha-Kruczynski M, McCann E, Fal'ko VI (2010) Electron-hole asymmetry and energy gaps in bilayer graphene. Semicond Sci Technol 25:033001
100. Vojta M, Fritz L, Bulla R (2010) Gate-controlled Kondo screening in graphene: quantum criticality and electron-hole asymmetry. EPL 90:27006
101. Itoh K, Takui T (2004) High spin chemistry underlying organic molecular magnetism. Topological symmetry rule as the first principle of spin alignment in organic open-shell systems of Ï€-conjugation and their ions. Proc Japan Acad Ser B 80:29–40
102. Kemp M, Roitberg A, Mujica V, Wanta T, Ratner MA (1996) Molecular wires: extended coupling and disorder effects. J Phys Chem 100:8349–8355
103. Reimers JR, Hush NS (1990) Electron and energy transfer through bridged systems. VII. Electronically-forbidden but vibronically-allowed long-range transfer: a case study using norbornylog bridges. Chem Phys 146:105
104. Wolfgang J, Risser SM, Priyadarshy S, Beratan DN (1997) Secondary structure conformations and long range electronic interactions in oligopeptides. J Phys Chem B 101:2986–2991
105. Bixon M, Jortner J (1997) Electron transfer via bridges. J Chem Phys 107:5154–5170
106. Balabin IA, Onuchic JN (2000) Dynamically controlled protein tunneling paths in photosynthetic reaction centers. Science 290:114–117
107. Troisi A, Ratner MA, Nitzan A (2003) Vibronic effects in off-resonant molecular wire conduction. J Chem Phys 118:6072–6082
108. Goldsmith RH, Wasielewski MR, Ratner MA (2006) Electron transfer in multiply bridged donor-acceptor molecules: Dephasing and quantum coherence. J Phys Chem B 110:20258–20262
109. Gagliardi A, Solomon GC, Pecchia A, Frauenheim T, Di Carlo A, Hush NS, Reimers JR (2007) A priori method for propensity rules for inelastic electron tunneling spectroscopy of single-molecule conduction. Phys Rev B 75:174306/1–174306/8
110. Skourtis SS, Waldeck DH, Beratan DN (2004) Inelastic electron tunneling erases coupling-pathway interferences. J Phys Chem B 108:15511–15518
111. Andrews DQ, Van Duyne RP, Ratner MA (2008) Stochastic modulation in molecular electronic transport junctions: molecular dynamics coupled with charge transport calculations. Nano Lett 8:1120–1126
112. Xiao D, Skourtis SS, Rubtsov IV, Beratan DN (2009) Turning charge transfer on and off in a molecular interferometer with vibronic pathways. Nano Lett 9:1818–1823
113. Skourtis SS, Waldeck DH, Beratan DN (2010) Fluctuations in biological and bioinspired electron-transfer reactions. Ann Rev Phys Chem 61:461–485
114. Landauer R (1957) Spatial variation of currents and fields due to localized scatterers in metallic conduction. IBM J Res Dev 1:223–231

115. Buttiker M, Imry Y, Landauer R, Pinhas S (1985) Generalized man-channel conductance formula with application to small rings. Phys Rev B 31:6207–6215
116. Meir Y, Wingreen NS (1992) Landauer formula for the current through an interacting electron region. Phys Rev Lett 68:2512–2515
117. Data S (1997) Electronic transport in mesoscopic systems. Cambridge University Press, Cambridge
118. Cuevas JC, Scheer E (2010) Molecular electronics: an introduction to theory and experiment. World Scientific, Singapore
119. Pauly F, Viljas JK, Huniar U, Häfner M, Wohlthat S, Bürkle M, Cuevas JC, Schön G (2008) Cluster-based density-functional approach to quantum transport through molecular and atomic contacts. New J Phys 10:125019
120. Solomon GC, Reimers JR, Hush NS (2005) Overcoming computational uncertainties to reveal chemical sensitivity in single molecule conduction calculations. J Chem Phys 122:224502-1–224502-7
121. Priyadarshy S, Skourtis SS, Risser SM, Beratan DN (1996) Bridge-mediated electronic interactions: differences between Hamiltonian and Green function partitioning in a non-orthogonal basis. J Chem Phys 104:9473–9481
122. Kurnikov IV, Beratan DN (1996) Ab initio based effective Hamiltonians for long-range electron transfer: Hartree-Fock analysis. J Chem Phys 105:9561–9573
123. Wang J, Guo H (2009) Relation between nonequilibrium Green's function and Lippmann-Schwinger formalism in the first-principles quantum transport theory. Phys Rev B 79:045119
124. Solomon GC, Herrmann C, Hansen T, Mujica V, Ratner MA (2010) Exploring local currents in molecular junctions. Nature Chem 2:223
125. Weinberg S (1995) The quantum theory of fields. Cambridge University Press, London
126. Crayston JA, Devine JN, Walton JC (2000) Conceptual and synthetic strategies for the preparation of organic magnets. Tetrahedron 56:7829–7857
127. Rajca A, Utamapanya S (1993) Toward organic synthesis of a magnetic particle: dendritic polyradicals with 15 and 31 centers for unpaired electrons. J Am Chem Soc 115:10688–10694
128. Rajca A, Rajca S, Wongsriratanakul J (1999) Very high-spin organic polymer: pi-conjugated hydrocarbon network with average spin of S >=40. J Am Chem Soc 121:6308–6309
129. Rajca A, Wongsriratanakul J, Rajca S (2001) Magnetic ordering in an organic polymer. Science 294:1503–1505
130. Mataga N (1968) Possible "ferromagnetic states" of some hypothetical hydrocarbons. Theor Chim Acta 10:372–376
131. Wohlthat S, Pauly F, Reimers JR (2008) The conduction properties of alpha-omega-diaminoalkanes and hydrazine bridging gold electrodes. Chem Phys Lett 454:284–288
132. Frisch MJ, Trucks GW, Schlegel HB et al (2009) Gaussian 09, revision A.02. Gaussian, Inc, Pittsburgh
133. Ahlrichs R, Bär M, Häser M, Horn H, Kölmel C (1989) Electronic structure calculations on workstation computers: the program system turbomole. Chem Phys Lett 162:165
134. TURBOMOLE V6.0 (2009) University of Karlsruhe and Forschungszentrum Karlsruhe GmbH, Karlsruhe
135. Wohlthat S, Kirchner T, Reimers JR (2009) N-silylamine junctions for molecular wires to gold: the effect of binding atom hybridization on the electronic transmission. J Phys Chem C 113:20458–20462
136. Zeng J, Hush NS, Reimers JR (1996) Solvent effects on molecular and ionic spectra. VII: Modeling the absorption and electroabsorption spectra of pentaammineruthenium(II)-pyrazine and its conjugate acid in water. J Am Chem Soc 118:2059
137. Shapley WA, Reimers JR, Hush NS (2002) INDO/S parameters for gold. Int J Quant Chem 90:424